Journal of Solid State Electrochemistry (2022) 26:959–971
https://doi.org/10.1007/s10008-022-05136-8

ORIGINAL PAPER

Flower-like titanium dioxide as novel co-reaction accelerator for ultrasensitive "off–on" electrochemiluminescence aptasensor construction based on 2D g-C_3N_4 layer for thrombin detection

Yu Lin[1] · Yeyu Wu[1] · Xuecai Tan[1] · Jiawen Wu[1] · Kejing Huang[1] · Yan Mi[1] · Panpan Ou[1] · Fucun Wei[1]

Received: 5 January 2022 / Revised: 10 February 2022 / Accepted: 10 February 2022 / Published online: 17 February 2022

Abstract

An ultrasensitive "signal-off–on" electrochemiluminescence (ECL) biosensor is constructed based on f1-TiO_2/g-C_3N_4/PDA for thrombin detection. The flower-like titanium dioxide (f1-TiO_2) has a huge specific surface area, which can not only increase the capacity of 2D graphite-like carbon nitride (g-C_3N_4) layer, but also promote the action of coreactants, and the ECL intensity of the electrode modified with f1-TiO_2/g-C_3N_4/PDA is 3.5 times higher than the electrode modified with g-C_3N_4/PDA. The carboxylated thrombin aptamer (sDNA) is incubated onto the modified electrode by amide bond; then, the complementary strand of thrombin aptamer (tDNA) modified with ferrocene is connected to the electrode surface by complementary base pairing with sDNA. Due to the ferrocene can quench the ECL of g-C_3N_4, the ECL signal decreases, while the ECL signal is restored in the presence of the target thrombin (TB). When $K_2S_2O_8$ and H_2O_2 are used as a co-reactant, the ECL aptasensor for TB detection is constructed with a concentration variation from 10^{-11} to 10^{-5} M, which has a excellent sensitivity, and the detection limit is 8.9×10^{-12} M. It also shows good specificity, reproducibility, and stability. This novel ECL aptasensor has potential application in human thrombin assay.

Keywords Electrochemiluminescence · 2D graphite-like carbon nitride · Flower-like titanium dioxide · Aptamer · Thrombin

Introduction

Thrombin, a multifunctional serine protease, is a major procoagulant and anticoagulant stimulator, which plays an important role in vascular injury and various pathological activities such as thrombotic diseases, atherosclerosis, and tumors. Therefore, it is necessary to develop an effective method for thrombin detection with high selectivity and specificity. At present, the main detection methods of thrombin include fluorescence [1–3], colorimetry [4–6], electrochemical method [7–10], LC–MS/MS [11, 12], and SPR [13]. However, the detection time of these methods is longer and the pretreatment of samples is more complicated than electrochemiluminescence (ECL). ECL has attracted much attention for its advantages such as simple operation, low cost, fast detection speed, high sensitivity, and simple instrument.

Electrochemiluminescence (ECL) refers to the substance on the electrode surface that is excited by the power source and forms excited state products through electron transfer. The excited state products then release energy and return to the ground state in the form of luminescence, which has the characteristics of both electrochemistry and chemiluminescence. Since the discovery of ECL, its application has expanded from the initial conventional analysis of inorganic and organic matter to biological and medical fields [14–18]. Compared with other detection methods, ECL has many advantages. Firstly, the sensitivity is higher and the linear range is wider. Secondly, it neither needs external

✉ Xuecai Tan
gxunxctan@126.com

✉ Kejing Huang
kejinghuang@163.com

[1] School of Chemistry and Chemical and Engineering, Guangxi University for Nationalities, Guangxi Key Laboratory of Chemistry and Engineering of Forest Products, Guangxi Collaborative Innovation Center for Chemistry and Engineering of Forest Products, Key Laboratory of Guangxi Colleges and Universities for Food Safety and Pharmaceutical Analytical Chemistry, Nanning 530008, China

light source, nor is affected by optical factors such as scattered light, and the background interference is small. In addition, through electrochemical reaction, the original non-luminescent materials can be transformed into chemiluminescent materials, expanding the scope of the determination of substances.

Graphite phase nitrogen carbide (g-C_3N_4) is a kind of metal-free semiconductor nanocrystalline material, which mainly takes triazine ring or heptaazine ring as the basic structural unit. Through the combination of vanderwaals force between layers and C-N covalent bond within layers, a graphite-like two-dimensional layered structure is formed. G-C_3N_4 has long been used in photoelectrocatalysis due to its unique energy band structure, good biocompatibility, cheap raw materials, and simple preparation. It was not until 2012 that Chang ming Cheng [19] discovered that g-C_3N_4 could generate cathode ECL signal around 460 nm through electron transfer in the presence of co-reactant $K_2S_2O_8$ that g-C_3N_4 was first applied in ECL detection. The next year, Chang ming Cheng [20] found that g-C_3N_4 could generate anodic ECL signal under the co-reaction agent TEA. So far, g-C_3N_4 has been tracked and explored by many ECL researchers [21–23].

Because of the poor electrical conductivity of g-C_3N_4, its ECL luminescence efficiency and sensitivity are not high. Therefore, how to improve the luminescence performance of g-C_3N_4 is an important research direction. Flower-like titanium dioxide (fl-TiO_2) is an important semiconductor material with a three-dimensional petal-like structure on its surface. Compared with other morphologies of titanium dioxide (such as quantum dot, spherical, tubular, porous), it has a larger specific surface area, and its surface is rich in hydroxyl, which is easy to be functionalized, so it has attracted widespread attention [24]. In this study, fl-TiO_2 was prepared by solvothermal method to form dioxide microparticles or nanoparticles, which was highly ordered and petaloid. The carboxylated g-C_3N_4 and amino-rich polydopamine (PDA) were loaded on fl-TiO_2. Due to the large specific surface area of fl-TiO_2, more g-C_3N_4 could be loaded, so that the luminescence efficiency and ECL signal stability of g-C_3N_4 were significantly improved. An "signal off–on" electrochemiluminescence sensor based on fl-TiO_2/g-C_3N_4/PDA for ultra-sensitive detection of thrombin (TB) was constructed. Firstly, amino-functionalized fl-TiO_2/g-C_3N_4/PDA was modified onto the electrode as the ECL luminescent material and the substrate to fix the carboxylated sDNA, and tDNA was further captured by base complementary pairing with sDNA. At the moment, the cathodic signal of g-C_3N_4 was quenched by ferrocene in tDNA. In the presence of TB, tDNA can be shed off from the electrode surface due to the specific binding between thrombin and sDNA; thus, the ECL signal of g-C_3N_4 was restored. The change of ECL intensity (ΔI) was related to the concentration of thrombin, and this ECL adaptorsensor has been applied to detect thrombin in the serum samples with satisfied results. The sensor construction process and detection mechanism are shown in Scheme 1.

Experimental section

Materials and reagents

Melamine ($C_3H_6N_6$), dopamine hydrochloride ($C_8H_{11}NO_2$·HC, 98%), tetrabutyl titanate ($C_{16}H_{36}O_4Ti$, 99%), terephthalic acid ($C_8H_6O_4$, 99%), N-hydroxysuccinimide (NHS, 98%), and 1-ethyl-(3-dimethylaminopropyl) carbon diimine hydrochloride (EDC, 98%) were purchased from Aladdin (Shanghai, China). Lysozyme ($C_{125}H_{196}N_{40}O_{36}S_2$), human hemoglobin ($C_{13}H_{10}N_2O_2$), human immunoglobulin, proserum, bovine hemoglobin, and bovine serum albumin (BSA) were purchased from Solarbio Science & Technology Co., Ltd (Beijing, China). The oligonucleotides were obtained from Sangon Biotechnology Inc. (Shanghai, China), including sDNA and tDNA. Phosphate-buffered saline (PBS) at pH 7.4 was used to wash the electrode and prepare aptamer solutions. All the reagents were analytical grade unless otherwise stated. The serum samples provided by the Ruikang Hospital Affiliated to Guangxi University of Chinese Medicine were used for real sample analysis.

Aptamer for TB (sDNA): 5′-HOOC-$(CH_2)_6$-ATT TGG CCA ACC ACA CCA ACC-3′.

Complementary strand (tDNA): 3′-Fc-$(CH_2)_6$-GGT TGG TGT GGT TGG-$(CH_2)_6$-Fc-5′.

Apparatus

ECL was measured on an MPI-B multi-parameter electrochemiluminescence system (Xi'an Remax Electronic Science & Technology Co., Ltd., China). The Eelectrochemical workstation CHI440 (Shanghai Chenhua Instrument Co., Ltd., China) was used to perform the cyclic voltammetry (CV) detection. Electrochemical impedance spectroscopy (EIS) was performed by the PGSTAT128N Autolab potentiostat/galvanostat (The Netherlands). Scanning electron microscopy (SEM) was tested by SUPPRA 55 Sapphire (Carl Zeiss, Germany); transmission electron microscopy (TEM) was tested by Tecnai F30 (FEI, USA), which were used to characterize the morphology of the materials. D8 ADVANCE X-ray powder diffractometer (AXS, Germany), Nicolet iS10 Fourier transform infrared spectrometer (Thermo Fisher Scientific, USA), UV-2100 UV–vis spectrophotometer (Beijing Beifen Ruili Co., Ltd., China), and FL-4600 fluorescence spectrometer (Hitachi, Japan) were utilized to characterize the experimental materials,

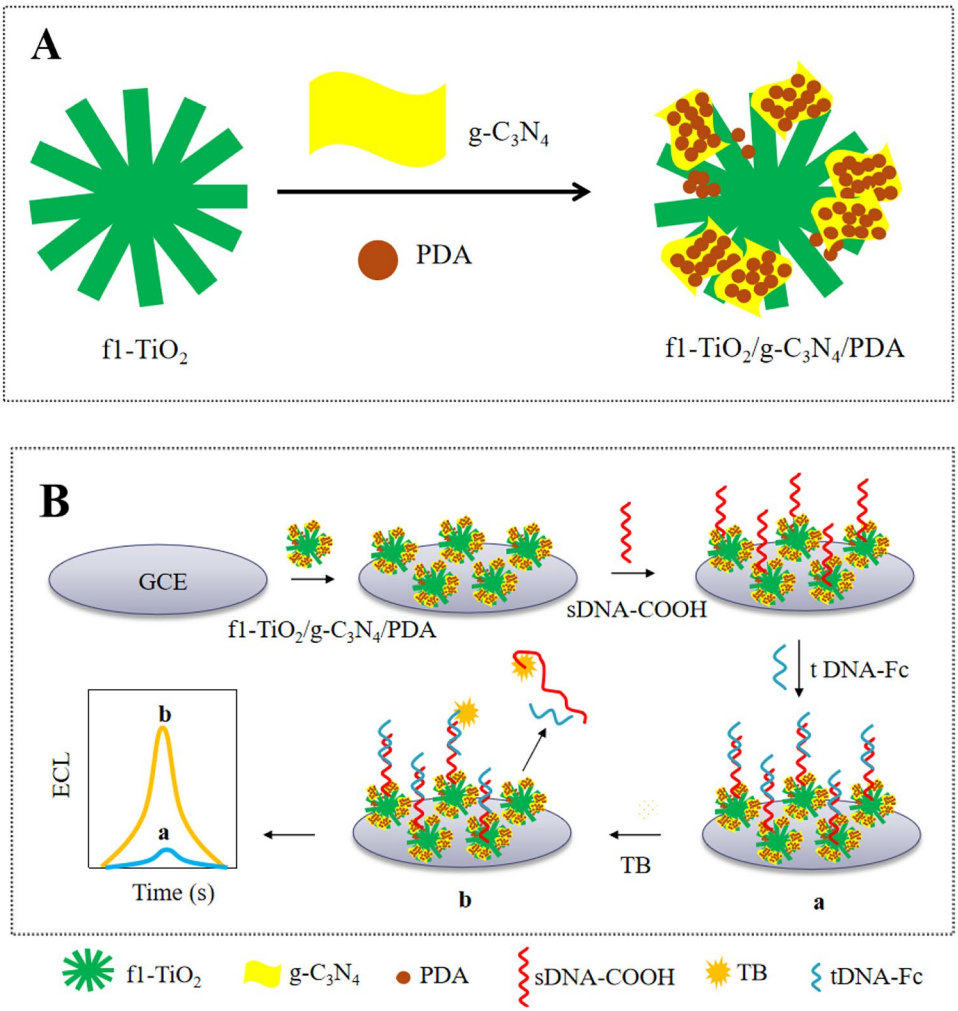

Scheme 1 Schematic representation of synthesis of fl-TiO_2/g-C_3N_4/PDA **A** and possible detection mechanism of the sensor **B**

respectively. Deionized water was taken from Milli-Q water purification system (Millipore, USA).

ECL, CV, and EIS detection were performed in the three-electrode system; the working electrode was modified glassy carbon electrode (GCE), the counter electrode was platinum pole, and the reference electrode was Ag/AgCl (sat. KCl) electrode or saturated calomel electrode (SCE). The scanning ranges of ECL potential detection and CV detection were − 1.8 ~ 0 V and − 0.2 ~ 0.6 V, respectively. The scan rates of ECL detection was 200 mV/s, and the scan rates of CV detection was 100 mV/s.

Preparation of materials

According to the literature [25, 26], carboxylate g-C_3N_4 was prepared by high temperature calcination polymerization. A total of 5.0 g of melamine powder was heated at 550 °C with a heating rate of 3 °C/min and kept for 4 h at this temperature. The yellow g-C_3N_4 product was ground to powder after naturally cooling to room temperature. Exactly 1.0 g of g-C_3N_4 powder was dispersed in 100 mL of 5 M HNO_3, which was refluxed at 125 °C for 24 h. After being centrifuged, washed down, and dried, carboxylated g-C_3N_4 powder was obtained. Carboxylated g-C_3N_4 powder was dispersed into distilled water and was performed by ultrasound for 16 h. In order to remove the residual unexfoliated g-C_3N_4, initial formed suspension was centrifuged at 5000 rmp. The collected supernatant was concentrated at 60 °C under reduced pressure, resulting in a milk-like suspension with the concentration about 1 mg/mL.

The polydopamine (PDA) was prepared by the self-polymerization of dopamine hydrochloride at room temperature for 24 h under magnetic stirring, and the pH of the suspension was adjusted to 8.5 by adding tris(hydroxymethyl) aminomethane [27]. After the unpolymerized DA was removed by centrifugation, the brown solid PDA was obtained, which was vacuum-dried for 12 h at 60 °C.

In a Teflon lined autoclave of 50 mL capacity, 2 mL of concentrated HCl solution was added dropwise into 4 mL of titanium butoxide; then, 20 mL of oleic acid was added and stirred at room temperature for 3 h; subsequently, the mixed solution was heated to 180 °C and kept for 12 h [28].

After natural cooling, the products were dried at 70 °C in vacuum, which were collected after washing with ethanol and hydrochloric acid repeatedly. Finally, the flower-like titanium dioxide (f1-TiO_2) was obtained by annealing.

For the preparation of fl-TiO_2/g-C_3N_4/PDA, 0.5 mg of PDA and 100 mg of f1-TiO_2 were added into 100 mL of 1 mg/mL carboxylate g-C_3N_4 under magnetic stirring 12 h at room temperature.

Fabrication and analytical procedure of the ECL aptasensor

Before modifying the electrodes, the bare GCE was polished with 1.0, 0.3, and 0.05 μm Al_2O_3 slurry successively, then was cleaned by 1:1 nitric acid, ethanol, and ultrapure water in turn. Subsequently, The GCE was modified by 4 μL of 1 mg/mL f1-TiO_2/g-C_3N_4/PDA dried at room temperature. And then, 600 μL EDC (45 mM) and NHS (15 mM) were added to sDNA (400 μL, 5 μM) solution to activate the carboxyl groups for 2 h. Next, 10 μL of activated sDNA was dropped on the modified electrode and incubated at 4 °C overnight. The unlinked sDNA was removed by washing with PBS, then BSA (10 μL, 1%) was dropped onto the modified electrode and incubated for 1 h so as to unbound active site. After that, tDNA (15 μL, 2 μM) was dropped onto the modified electrode and incubated for 2 h, and then rinsed with PBS. Finally, the aptasensor was constructed successfully.

Different concentrations of thrombin (10 μL) were incubated on the surface of f1-TiO_2/g-C_3N_4/PDA/GCE at room temperature for 1 h, and then, the electrode was washed with PBS solution (0.1 M, pH 7.4). The ECL response of the aptasensor was detected in PBS containing 0.1 M $K_2S_2O_8$ and H_2O_2. The scan voltage range, photomultiplier voltage, and scan rate were − 1.8 ~ 0 V, 400 V, and 200 mV/s, respectively.

Results and discussion

Characterization of the synthesized materials

The morphology of different materials was characterized by scanning electron microscopy (SEM) and transmission electron microscopy (TEM). As shown in Fig. 1A, f1-TiO_2 was a flower-like structure with a particle size of 5 μm. Figure 1B is the SEM image of f1-TiO_2/g-C_3N_4/PDA composite material, which inner illustration in the bottom right-hand corner was the microgram, indicating that g-C_3N_4 loaded with PDA was distributed on the surface of f1-TiO_2. The TEM image of Fig. 1C showed that g-C_3N_4 was a two-dimensional sheet with 3-nm thickness. The TEM result of Fig. 1D proved the composites of f1-TiO_2/g-C_3N_4/PDA were prepared successfully.

Figure 2A showed the FT-IR spectra of g-C_3N_4 NSs. The uncondensed -NH_2 and = NH groups at the edge of CN heterocyclic polymer were located at the wide peak between

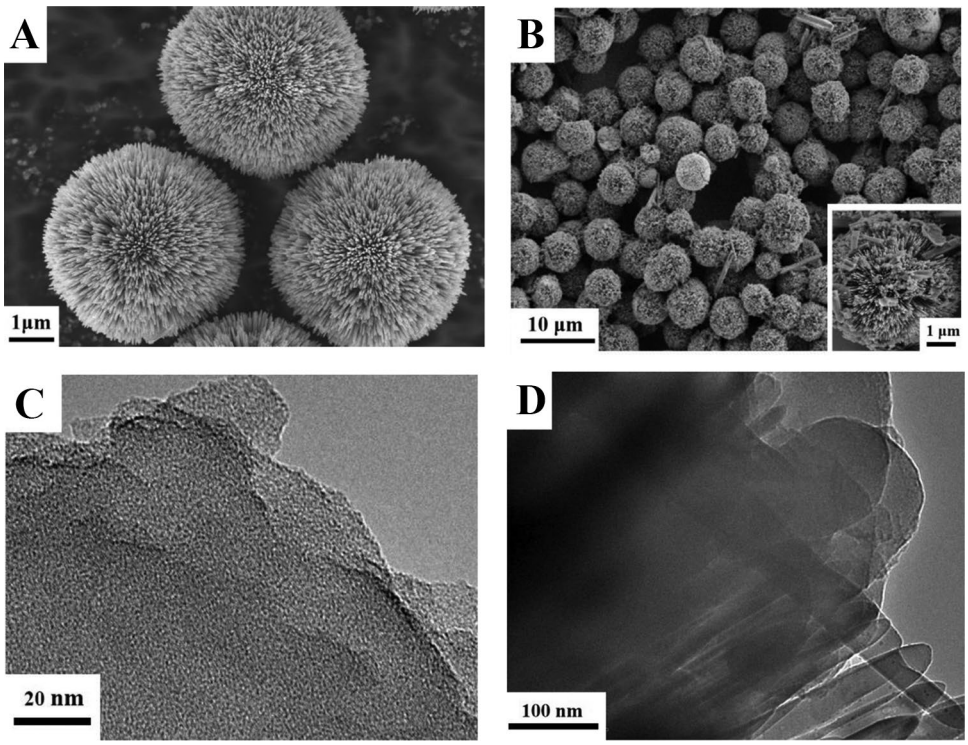

Fig. 1 SEM images of **A** f1-TiO_2 and **B** f1-TiO_2/g-C_3N_4/PDA; TEM images of **C** g-C_3N_4 and **D** f1-TiO_2/g-C_3N_4/PDA

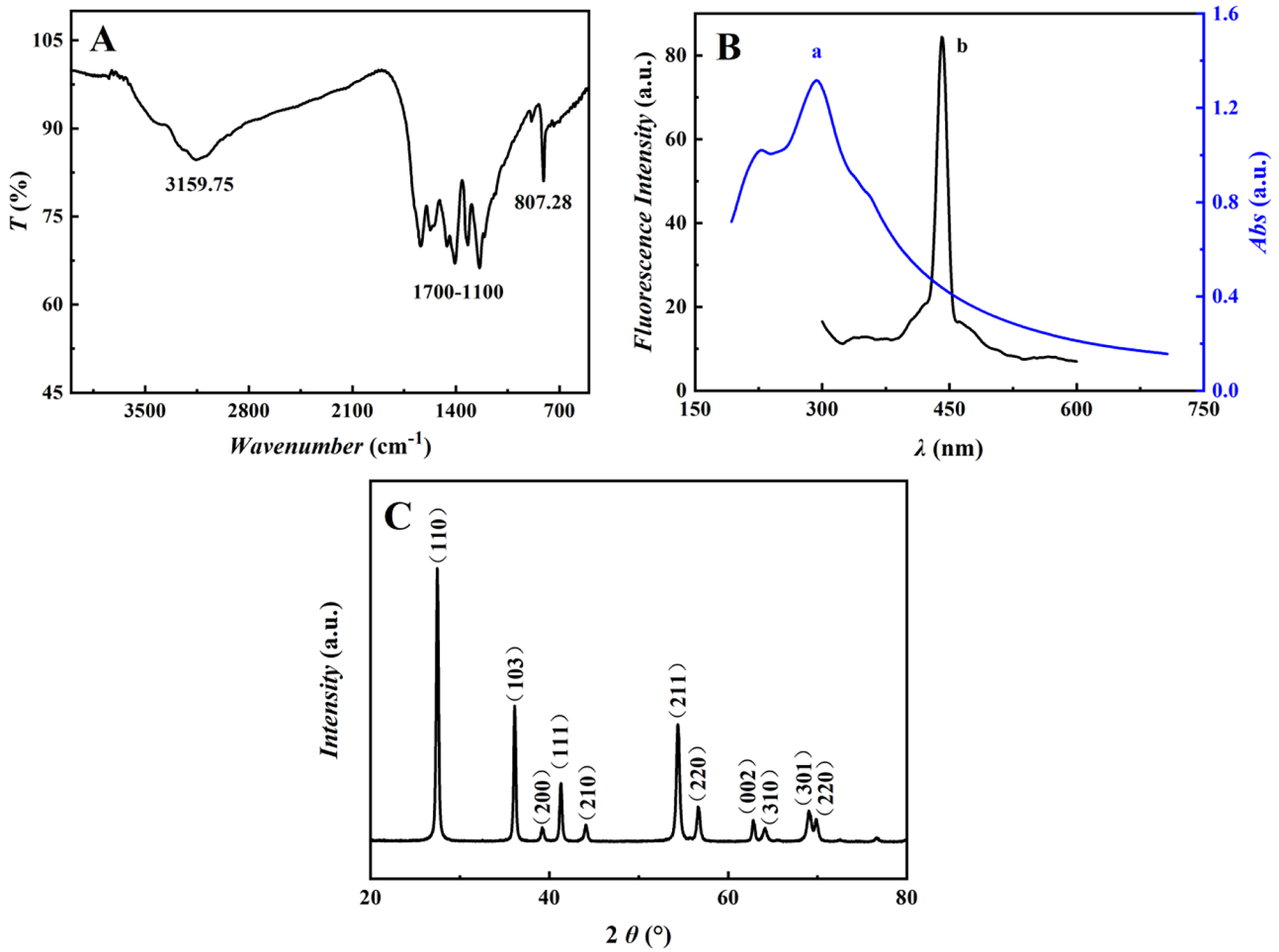

Fig. 2 **A** Infrared spectrogram (IR)of g-C_3N_4, **B** ultraviolet **a** and fluorescence **b** spectra of g-C_3N_4, and **C** X-ray diffraction (XRD) of fl-TiO_2

3000 and 3500 cm^{-1}. The peak of 1700 cm^{-1} was attributed to C = O stretching. The absorption bands between 1100 and 1600 cm^{-1} were corresponding to either triangular N-$(C)_3$ or bridging C-NH-C units. The sharp peak located at 807 cm^{-1} was associated with triazine ring vibrations. All these indicated the successful functionalization of carboxyl group on g-C_3N_4 NSs [29–31]. The results of Fig. 2B were consistent with the references [29, 32]; the ultraviolet characteristic spectrum of g-C_3N_4 was at 320 nm (Fig. 2B (a)), which was taken as the excitation wavelength of the fluorescence spectrum; meanwhile, g-C_3N_4 produced fluorescence emission at 440 nm (Fig. 2B (b)). According to the XRD patterns (Fig. 2C), the pattern of fl-TiO_2 almost corresponded to crystal planes of anatase TiO_2 (JCPDS No. 21–1272), and the identical peaks at $2\theta = 69.9°$ and 36.3°, which represented (220) and (103) crystal planes, respectively. Moreover, the main diffraction peaks of fl-TiO_2 at 27.6°, 39.4°, 41.5°, 44.2°, 54.5°, 56.8°, 62.9°, 64.3°, and 69.2° were indexed to (110), (200), (111), (210), (211), (220), (002), (310), and (301) crystal planes of rutile phase TiO_2 (JCPDSNO. 21–1276), respectively. The results of Fig. 2C indicated that fl-TiO_2 was a mixed crystal composed of anatase and rutile phases.

According to X-ray photoelectron spectroscopy (XPS) spectrum of Fig. 3, the chemical composition of f1-TiO_2/g-C_3N_4 surface was characterized. The C 1S XPS spectrum was shown in Fig. 3A; two peaks appeared at 284.58 eV and 287.99 eV, respectively. The peak located at 284.58 eV was contributed to the sp peak of carbon atom, and another peak located at 287.99 eV implied that carbon atoms had one double bond and two single bonds with three neighbor N atoms. As shown in Fig. 3B, the peak at 398.57 eV and 400.78 eV were obtained after Gaussian curve fitting, which were attributed to C = N–C and N-$(C)_3$. Meanwhile, the N-$(C)_3$ group in N 1S XPS spectrum demonstrated the polymerization of melamine [33]. The XPS peak of Ti $2p_{3/2}$ and Ti $2p_{1/2}$ were at 458.33 eV and 464.28 eV in Fig. 3C, respectively. The differentiation of Ti $2p_{3/2}$ and Ti $2p_{1/2}$ was about 5.95 eV, indicating the typical characteristic of Ti^{4+} were found in f1-TiO_2 [34, 35]. The O 1 s spectrum in Fig. 3D

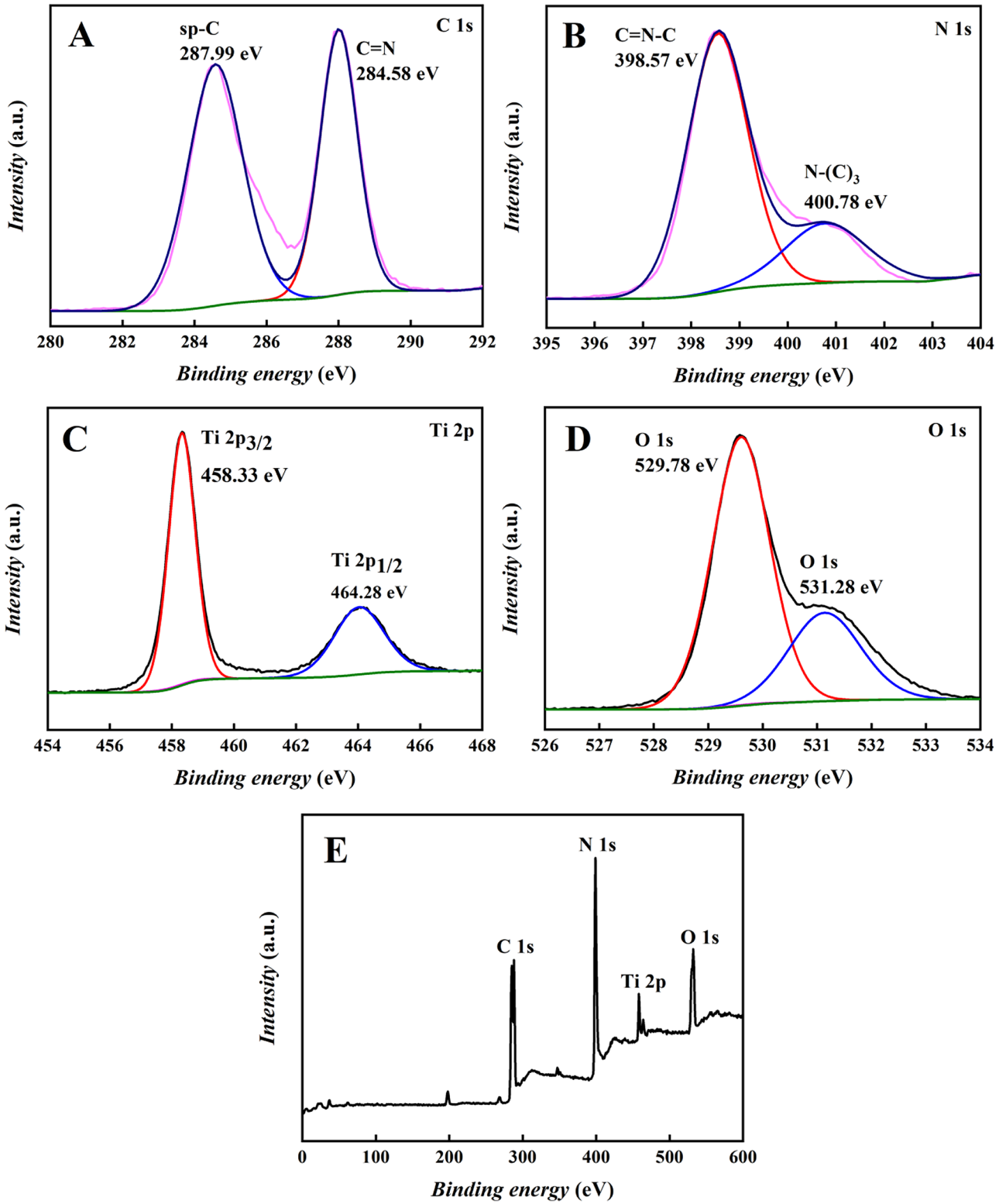

Fig. 3. XPS analysis of f1-TiO_2/g-C_3N_4 composite material: **A** C 1 s, **B** N 1 s, **C** Ti 2p, **D** O 1 s, **E** survey scans

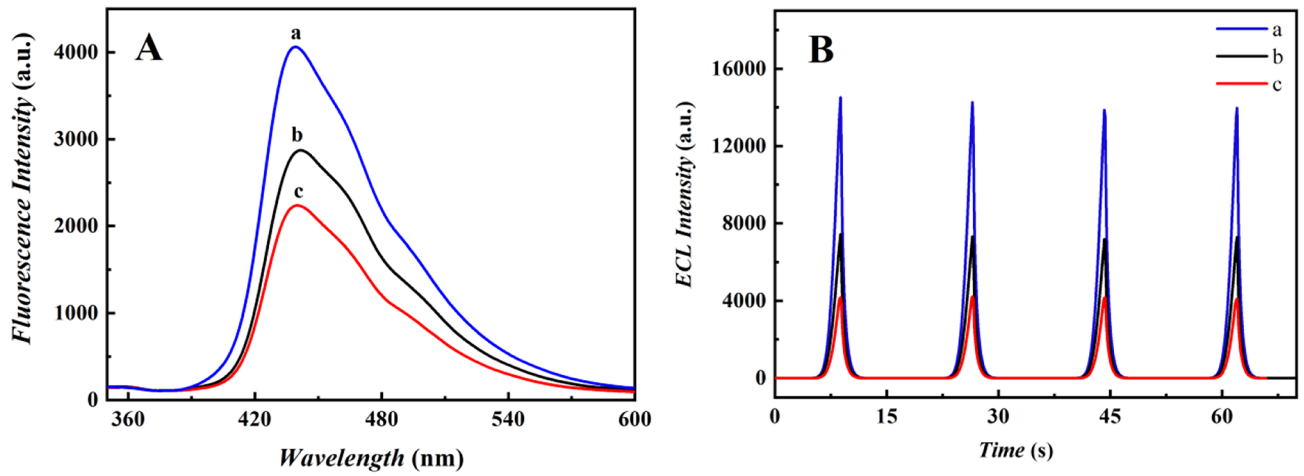

Fig. 4 Fluorescence spectra **A** and ECL behavior **B** of various materials: **a** f1-TiO_2/g-C_3N_4/PDA, **b** g-C_3N_4, and **c** g-C_3N_4/PDA

displayed two peaks located at 529.78 eV and 531.28 eV. The characteristic peak of binding energy 529.78 eV corresponded to Ti–O bond in TiO_2, and the peak of 531.28 eV can be attributed to C–O bond [36]. Figure 3E showed the XPS full-scan spectra of f1-TiO_2/g-C_3N_4, and the typical elements of C, N, Ti, and O were indicated. The results of XPS proved the g-C_3N_4 was growed on the surface of f1-TiO_2 nanoflower successfully.

The verification of catalysis of flower-like titanium dioxide

Figure 4A showed the fluorescence emission spectra of different materials, indicating that PDA can absorb the fluorescence emitted of g-C_3N_4 [37]. As a result, the fluorescence intensity of g-C_3N_4/PDA composite material (Fig. 4A (c)) was lower than that of g-C_3N_4 single material (Fig. 4A (b)), and f1-TiO_2 could restore and enhance the fluorescence intensity of g-C_3N_4 (Fig. 4A (a)). In addition, under the same detection conditions, the ECL intensity of f1-TiO_2/g-C_3N_4/PDA was 3.5 times as large as g-C_3N_4/PDA, shown as Fig. 4B. Thus, f1-TiO_2 was selected as the catalyst of the luminescence system.

Electrochemical behavior of the modified electrode

The electrochemical behavior on different modified electrodes was investigated by cyclic voltammetry (CV), which was shown in Fig. 5A. The surface properties of the electrode were investigated by electrochemical impedance

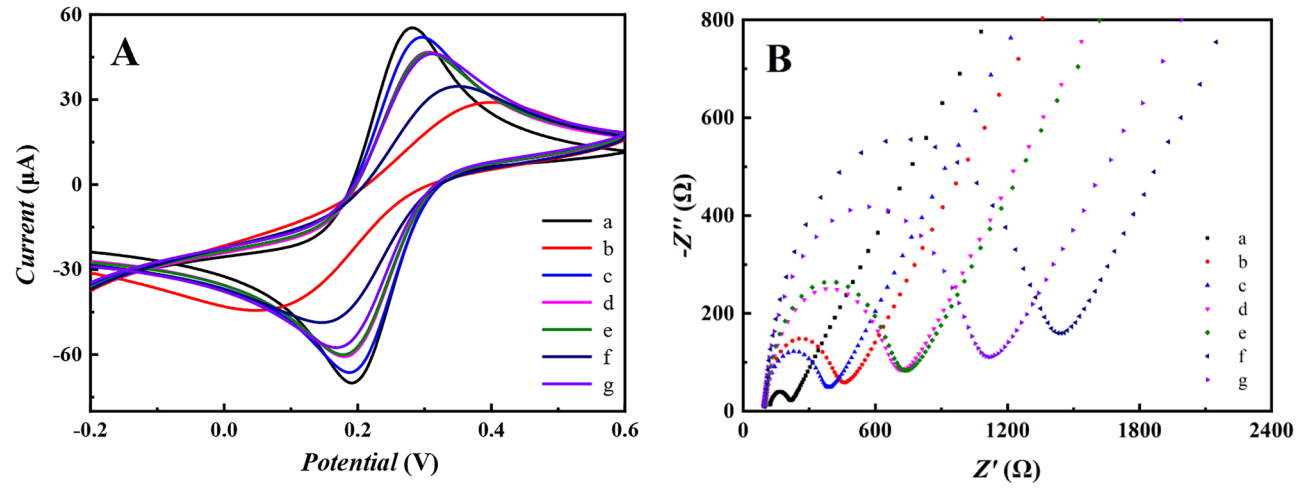

Fig. 5 Cyclic voltammetry **A** and electrochemical impedance spectroscopy **B** of various materials: **a** bare GCE, **b** g-C_3N_4, **c** f1-TiO_2/g-C_3N_4/PDA, **d** f1-TiO_2/g-C_3N_4/PDA + sDNA, **e** f1-TiO_2/g-C_3N_4/PDA + sDNA + BSA, **f** f1-TiO_2/g-C_3N_4/PDA + sDNA + BSA + tDNA, and **g** f1-TiO_2/g-C_3N_4/PDA + sDNA + BSA + tDNA + TB

spectroscopy (EIS). A total of 5 mM $[Fe(CN)_6]^{3-/4-}$ containing 0.1 M KCl was used as a redox probe, as shown in Fig. 5B. Compared with the bare GCE (curve a), due to the poor conductivity of g-C_3N_4, the g-C_3N_4 modified electrode (curve b) showed smaller current and larger impedance. Because of the excellent electron transport of f1-TiO_2, the current (curve c) became larger and the impedance became smaller compared with the g-C_3N_4 (curve b), when the GCE was modified with f1-TiO_2/g-C_3N_4/PDA. Because sDNA and BSA were weakly conductive macromolecular which hindered the electron transfer, so that the f1-TiO_2/g-C_3N_4/PDA/sDNA modified electrode (curve d) and the f1-TiO_2/g-C_3N_4/PDA/sDNA/BSA modified electrode (curve e) showed smaller current and larger impedance. According to the base complementary pairing principle, when the electrode modified with f1-TiO_2/g-C_3N_4/PDA/sDNA/BSA was incubated by tDNA, the current became smaller and the impedance became larger, because the electrochemiluminescence of g-C_3N_4 can be quenched by the ferrocene in tDNA and electron transfer was blocked, shown as Fig. 5 curve f. In the presence of thrombin, tDNA would follow sDNA falling off from the electrode surface into solution, due to the specific binding between thrombin and sDNA. As the obstructions on the electrode surface decreased, the current increased and the impedance decreased as Fig. 5 curve g.

ECL spectra of different electrodes were investigated in 0.1 M $K_2S_2O_8$ containing H_2O_2 (Fig. 6). The results showed that f1-TiO_2/g-C_3N_4/PDA (curve a) had a strong ECL signal. Because of the ECL resonance energy transfer (ERET) between g-C_3N_4 and the ferrocene groups located in tDNA, the ECL signal on the electrode surface modified with f1-TiO_2/g-C_3N_4/PDA /sDNA/BSA/tDNA (curve c) was reduced. In the presence of thrombin, the binding strength between thrombin and sDNA was greater than the base-pairing binding strength between sDNA and tDNA, so tDNA was dragged away from the electrode surface. As a result (curve b), the ERET interaction was weakened and the ECL signal was recovered.

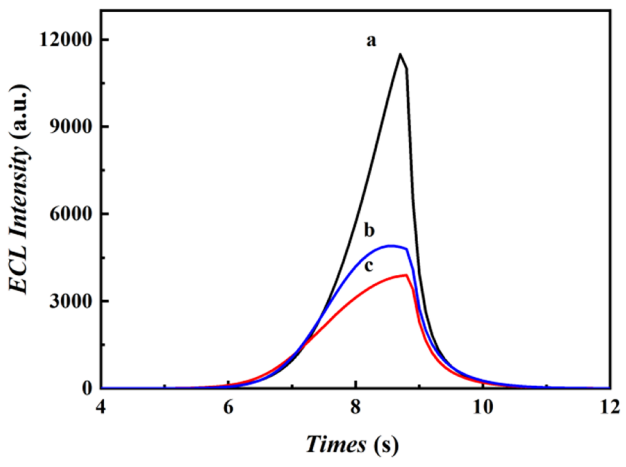

Fig. 6 Electrochemiluminescence of different electrodes: **a** f1-TiO_2/g-C_3N_4/PDA, **b** f1-TiO_2/g-C_3N_4/PDA + sDNA + BSA + tDNA + TB, and **c** f1-TiO_2/g-C_3N_4/PDA + sDNA + BSA + tDNA

Mechanism of the ECL system

The cathode ECL signal can be generated by g-C_3N_4 with $K_2S_2O_8$ as co-reactant at the voltage of − 1.8 ~ 0 V. When suitable dosage of 0.03 M H_2O_2 was added into 0.1 M $K_2S_2O_8$, the ECL signal of g-C_3N_4 can be enhanced. Following the increasement of 0.03 M H_2O_2 dosage, g-C_3N_4 would appear double peaks and its stability would deteriorate. Therefore, 0.1 M $K_2S_2O_8$ and appropriate amount of H_2O_2 were selected as the co-reactant for the system. As an important metal oxide semiconductor, titanium dioxide has valence band–dependent catalytic performance and can promote the generation of reactive oxygen species, such as OH^*. The flower-like titanium dioxide (f1-TiO_2) can catalyze the decomposition of hydrogen peroxide to a greater extent, which has a larger specific surface area. The reaction mechanism is showed as the follow equations [38–40]:

$$g - C_3N_4 + e^- \rightarrow g - C_3N_{4^-} \quad (1)$$

$$H_2O_2 + e^- \rightarrow OH^- + OH^* \quad (2)$$

$$OH^* + g - C_3N_{4^-} \rightarrow g - C_3N_{4^-} + OH^- \quad (3)$$

$$S_2O_{8^{2-}} + e^- \rightarrow SO_{4^{2-}} + SO_{4^-} \quad (4)$$

$$g - C_3N_{4^-} + SO_{4^-} \rightarrow g - C_3N_{4^*} + SO_{4^{2-}} \quad (5)$$

and/or

$$g - C_3N_4 + SO_{4^-} \rightarrow g - C_3N_{4^+} + SO_{4^{2-}} \quad (6)$$

$$g - C_3N_{4^+} g - C_3N_{4^-} \rightarrow g - C_3N_{4^*} + g - C_3N_4 \quad (7)$$

finally,

$$g - C_3N_{4^*} \rightarrow g - C_3N_4 + hv \quad (8)$$

Optimization of experimental parameters

The electrochemical luminescence performance of 1 mg/mL f1-TiO_2/g-C_3N_4/PDA with different modification amounts was investigated, and the results were shown in Fig. 7A. With the increment of $V_{\text{f1-TiO2/g-C3N4/PDA}}$, the ECL strength of the system augmented. When $V_{\text{f1-TiO2/g-C3N4/PDA}} \geq 4$ μL, the ECL signal reached the maximum and was basically stable. Therefore, 4 μL of 1 mg/mL f1-TiO_2/g-C_3N_4/PDA was modified to the electrode surface for experiment.

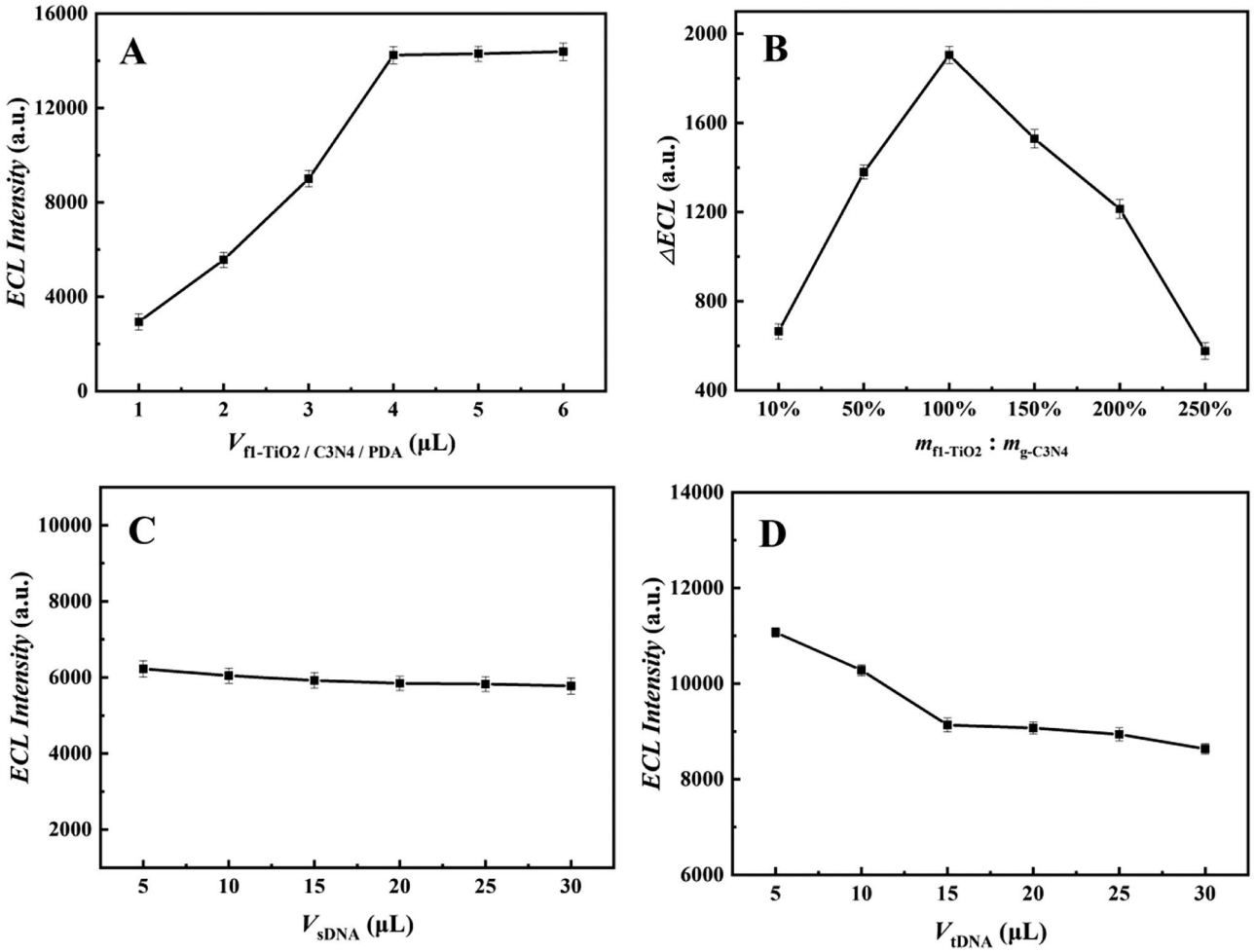

Fig. 7 **A** Optimization of f1-TiO_2/g-C_3N_4/PDA coating amount, **B** optimization of f1-TiO_2 coating amount, **C** optimization of sDNA coating amount, and **D** optimization of tDNA coating amount

The influences of different dosages of f1-TiO_2 on the experiment were investigated, and Fig. 7B was obtained. When $m_{\text{f1-TiO2}}$:$m_{\text{g-C3N4}} \leq 100\%$, the luminescence of g-$C_3N_4$ could be promoted with the increase of the dosage of f1-TiO_2. However, when $m_{\text{f1-TiO2}}$:$m_{\text{g-C3N4}} > 100\%$, with the increased dosage of f1-TiO_2, partial luminescence sites of g-C_3N_4 were blocked, ΔI_{ECL} decreased. Therefore, the addition amount of f1-TiO_2 in the composite material was selected the same as that of g-C_3N_4.

The influence of 2 μM sDNA with different modification amounts on the sensor was explored, and the result is shown in Fig. 7C. Although sDNA was macromolecular nucleotide, which would cover the sectional chemiluminescence sites of g-C_3N_4, resulting in the decrease of the ECL signal of g-C_3N_4, due to the concentration and dosage of sDNA were low, the ECL of g-C_3N_4 did not change significantly with the increase of sDNA. Considering incubation temperature and time, 10 μL of sDNA was selected.

The effect of tDNA dosage on sensor performance was investigated. Because the ECL signal of g-C_3N_4 was quenched by ferrocene, thus, I_{ECL} decreased with the increase of tDNA dosage, shown as Fig. 7D. When V_{tDNA} was 15 μL, the binding between tDNA and sDNA reached saturation, and the ECL signal of g-C_3N_4 decreased the most. When $V_{\text{tDNA}} > 15$ μL, though the chemiluminescence site of g-C_3N_4 was still blocked by tDNA, the reduction of ECL signal was as similar as that of the electrode modified with 15 μL tDNA. Therefore, 15 μL of tDNA was chosen to incubate the modified electrode.

Performance of the ECL aptasensor

Under optimal experimental conditions, different concentrations of thrombin were detected by this sensor. Shown as Fig. 8A, the ECL signal of the sensor increased gradually with the increase of thrombin concentration. The change

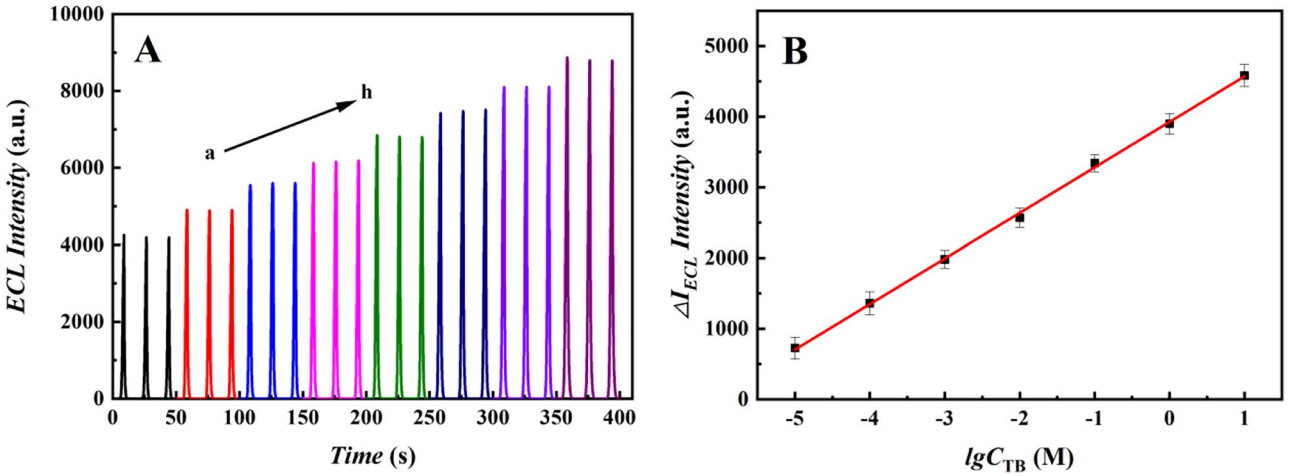

Fig. 8 **A** ECL response of the sensors in different concentrations of thrombin **a–h**: **a** 0 M, **b** 10^{-11} M, **c** 10^{-10} M, **d** 10^{-9} M, **e** 10^{-8} M, **f** 10^{-7} M, **g** 10^{-6} M, and **h** 10^{-5} M; **B** Calibration curve for thrombin detection ($N=3$)

of the ECL intensity (ΔI) presented a linear relationship with the logarithmic concentration of thrombin vary from 10^{-11} to 10^{-5} M (Fig. 8B), the linear equation was $\Delta I = 643.18 lgC + 7783.71$, R^2 was 0. 9989, and the detection limit was 8.9×10^{-12} M (S/N = 3). Compared with other methods for thrombin detection, the detection range of this sensor was wider, and detection limit was lower, as shown in Table 1.

As seen from Fig. 9A, seven different electrodes modified with f1-TiO_2/g-C_3N_4/PDA were constructed to detect TB (10^{-6} M) at the same dosage, respectively. The relative standard deviation (RSD) was 0.84% ($N=5$), indicating that the reproducibility of this ECL sensor was outstanding. In order to explore the stability of the sensor, the same modified electrode was used to detect the same amount of 10^{-6} M thrombin for 15 times; the RSD was 0.38% (Fig. 9B). In Fig. 9C, the same modified electrode was placed at 4 °C for 7 days, the ECL strength decreased by 4.84% compared with the first day, and the RSD was 1.86% ($N=5$); all of the above outcomes verify that the stability of this biosensor was good.

To evaluate the selectivity of the ECL aptasensor, different model interfering substances were selected, including lysozyme, human immunoglobulin (lg G), human albumi, hemoglobin, and bovine serum albumin (BSA). The concentration of thrombin was 10^{-7} M, while the concentration of interferences was 10^{-5} M. Figure 9D showed that the above interferers did not produce an obvious signal changes ($N=5$), which was compared with the blank experiment. On the contrary, the ECL strength of thrombin increased significantly when TB was present. Because of the specificity between TB and its aptamer, other proteins and enzymes cannot be captured on the electrode, so no signal change was observed significantly, indicating that the selectivity of this biosensor was perfect.

Real sample analysis

The human serum samples for real sample analysis were provided by Ruikang Hospital Affiliated to Guangxi University of Chinese Medicine. A total of 10^{-7} M, 10^{-8} M, and 10^{-9} M TB were added into the serum of normal people, respectively, and the determination results are shown in Table 2. The recoveries were 97.72–104.7%, and the RSDs were 1.06–2.13%, indicating that this ECL aptasensor had great potential for thrombin detection in real human samples.

Table 1 The comparison of other methods for determination of thrombin

Method	Linear range (M)	Detection limit (M)	Reference
Fluorescent	1.6×10^{-6}–8.0×10^{-6}	1.6×10^{-6}	[3]
Colorimetry	1.08×10^{-7}–2.7×10^{-5}	2.78×10^{-8}	[4]
LC–MS/MS	5.0×10^{-8}–1.0×10^{-5}	7.0×10^{-9}	[11]
SPR	1.0×10^{-6}–2.0×10^{-5}	1.1×10^{-6}	[13]
spICP-MS	1.0×10^{-11}–1.0×10^{-7}	4.5×10^{-12}	[41]
Photoelectrochemistry	1.0×10^{-8}–1.0×10^{-6}	5.0×10^{-11}	[42]
Electrochemistry	1.0×10^{-10}–1.0×10^{-5}	3.5×10^{-11}	[43]
Electrochemiluminescene	1.0×10^{-11}–1.0×10^{-5}	8.9×10^{-12}	This work

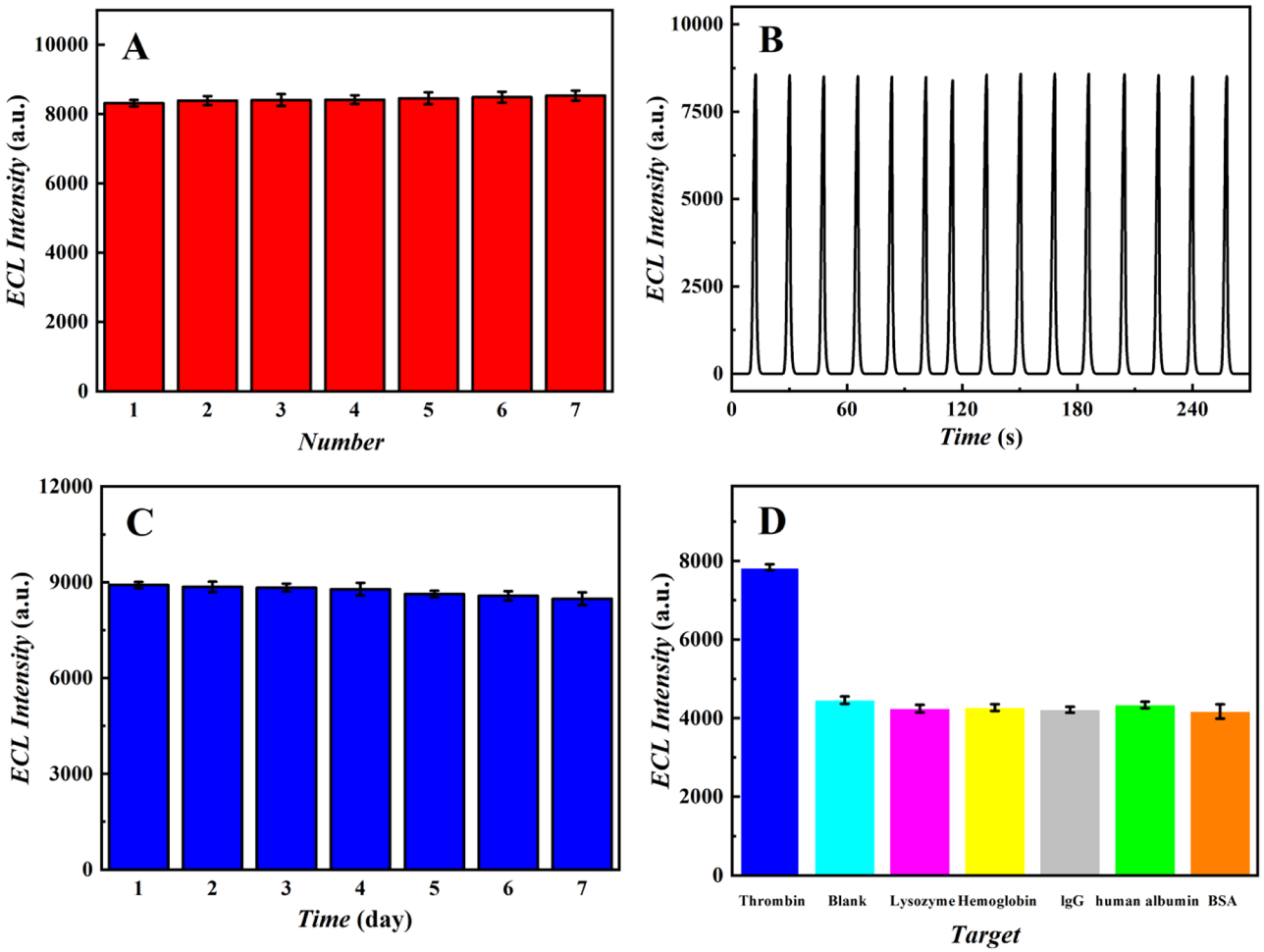

Fig. 9 Repeatability **A**, short-term stability **B**, long-term stability **C**, and selectivity **D** of the as-prepared sensor

Table 2 Determination and recovery of thrombin in normal human serum

Sample	Added (M)	Detected (M)	Recovery (%)	RSD (%)
1	1.000×10^{-7}	1.047×10^{-7}	104.7	1.32
2	1.000×10^{-8}	1.023×10^{-8}	102.3	1.06
3	1.000×10^{-9}	9.772×10^{-10}	97.72	2.13

Conclusions

In summary, a novel ECL sensor based on f1-TiO_2/g-C_3N_4/PDA is constructed for thrombin detection. The sensor presents good analytical performance including the low detection limit, high sensitivity, and excellent selectivity, which is successfully applied to determine thrombin in normal human serum. This study provides a new ECL signal amplification strategy, and broadens the application of ECL sensor in bioanalysis.

Funding This work was supported by the National Natural Science Foundation of China (Nos. 21365004, 22074130), the 2021 Guangxi Doctoral Innovation Project (YCBZ2021060), the Key Research and Development Project of Guangxi (AB18126048), Guangxi innovation-driven Development Special Fund project (AA18118013-10), the Specific Research Project of Guangxi for Research Bases and Talents (AD18126005), Young and middleaged teachers basic ability promotion project by Guangxi Education Department (2019KY0162), Innovation Project of Guangxi University for Nationalities Graduate Education (gxun-chxps202077), and Zhongyuan Thousand Talents Plan-Science and Technology Innovation Leading Talents Project (204200510030).

References

1. Cui HY, Fu XQ, Yang L, Xing S, Wang XF (2021) 2D titanium carbide nanosheets based fluorescent aptasensor for sensitive detection of thrombin. Talanta 228:122219. https://doi.org/10.1016/j.talanta.2021.122219
2. Zhang ZQ, Liu NN, Zhang ZC, Xu DY, Ma S, Wang XF, Zhou T, Zhang GD, Wang F (2021) Construction of aptamer-based molecular beacons with varied blocked structures and targeted

detection of thrombin. Langmuir 37(29):8738–8745. https://doi.org/10.1021/acs.langmuir.1c00994
3. Zhang BZ, Wei CY (2020) An aptasensor for the label-free detection of thrombin based on turn-on fluorescent DNA-templated Cu/Ag nanoclusters. RSC Adv 10:35374–35380. https://doi.org/10.1039/D0RA04609D
4. Shen MM, Wang YY, Kan XW (2021) Dual-recognition colorimetric sensing of thrombin based on surface-imprinted aptamer-Fe_3O_4. J Mater Chem B 9:4249–4256. https://doi.org/10.1039/D1TB00565K
5. Duan WN, Wang XZ, Wang HX, Li F (2018) Fluorescent and colorimetric dual-mode aptasensor for thrombin detection based on target-induced conjunction of split aptamer fragments. Talanta 180:76–80. https://doi.org/10.1016/j.talanta.2017.12.033
6. Liu M, Li J, Li BX (2017) A colorimetric aptamer biosensor based on cationic polythiophene derivative as peroxidase mimetics for the ultrasensitive detection of thrombin. Talanta 175:224–228. https://doi.org/10.1016/j.talanta.2017.07.003
7. Yang Y, Yao LY, Liang WB, Huang W, Zhang YJ, Zhang JL, Yuan R, Xiao DR (2021) Highly efficient electrochemiluminescence resonance energy transfer material constructed from an AIEgen-based 2D ultrathin metal-organic layer for thrombin detection. Chemcomm 57:4323–4326. https://doi.org/10.1039/D1CC00364J
8. Li W, Zhao D, Tian DD, Zhai MM, Xu HD, Zheng LC, Li SQ, Sang Y (2021) Electrochemical aptasensor based on proximity binding-induced DNA networked for enzyme-free and ultrasensitive detection of thrombin-ScienceDirec. J Electroanal Chem 895:115447. https://doi.org/10.1016/j.jelechem.2021.115447
9. Jamei HR, Rezaei B, Ensafi AA (2021) Ultra-sensitive and selective electrochemical biosensor with aptamer recognition surface based on polymer quantum dots and C60/MWCNTs-polyethylenimine nanocomposites for analysis of thrombin protein. Bioelectrochemistry 138:107701. https://doi.org/10.1016/j.bioelechem.2020.107701
10. Wang J, Song MM, Hu CG, Wu KB (2018) Portable, self-powered, and light-addressable photoelectrochemical sensing platforms using pH meter readouts for high-throughput screening of thrombin inhibitor drugs. Anal Chem 90(15):9366–9373. https://doi.org/10.1021/acs.analchem.8b01979
11. Li D, Song QX, Li TF, Shu C, Ji SL, Su C, Su YW, Ding L (2020) An LC-MS/MS method for protein detection based on a mass barcode and dual-target recognition strategy. RSC Adv 10(27):16094–16100. https://doi.org/10.1039/D0RA01783C
12. Shu C, Li TF, Li D, Li ZQ, Xia XH (2021) Barcode signal amplifying strategy for sensitive and accurate protein detection on LC-MS/MS. Analyst 146(5):1725–1733. https://doi.org/10.1039/D0AN01948H
13. Kotlarek D, Vorobii M, Ogieglo W, Knoll W, Emmenegger CR, Dostalek J (2019) Compact grating-coupled biosensor for the analysis of thrombin. ACS Sensors 4(8):2109–2116. https://doi.org/10.1021/acssensors.9b00827
14. Nikolaou P, Valenti G, Paolucci F (2021) Nano-structured materials for the electrochemiluminescence signal enhancement. Electrochim Acta 388:138586. https://doi.org/10.1016/j.electacta.2021.138586
15. Zhao CZ, Niu LL, Wang XY, Sun W (2020) A simple and convenient electrochemiluminescence immunoassay by using gold nanoparticles as both label and co-reactant. Bioelectrochemistry 135:107585. https://doi.org/10.1016/j.bioelechem.2020.107585
16. Ge L, Guo CX, Li H, Xia X, Chen LY, Ning DX, Liu XJ, Li F (2021) Direct-laser-writing of electrochemiluminescent electrode on glassy carbon for iodide sensing in aqueous solution. Sensors Actuat B-Chem 337:129766. https://doi.org/10.1016/j.snb.2021.129766
17. Feng DF, Wei FC, Wu YY, Tan XC, Li F, Lu YK, Fan GC, Han HY (2021) A novel signal amplified electrochemiluminescence biosensor based on MIL-53(Al)@CdS QDs and SiO2@AuNPs for trichlorfon detection. Analyst 146:1295–1302. https://doi.org/10.1039/D0AN02158J
18. Feng DF, Tan XC, Wu YY, Ai CH, Luo YN, Chen QY, Han HY (2019) Electrochemiluminecence nanogears aptasensor based on MIL-53(Fe)@CdS for multiplexed detection of kanamycin and neomycin. Biosens Bioelectron 129:100–106. https://doi.org/10.1016/j.bios.2018.12.050
19. Cheng CM, Huang Y, Tian XQ, Zheng BZ, Li Y, Yuan HY, Xiao D, Xie SP, Martin MFC (2012) Electrogenerated chemiluminescence behavior of graphite-like carbon nitride and its application in selective sensing Cu^{2+}. Anal Chem 84(11):4754–4759. https://doi.org/10.1021/ac300205w
20. Cheng CM, Huang Y, Wang J, Zheng BZ, Yuan HY, Xiao D (2013) Anodic electrogenerated chemiluminescence behavior of graphite-like carbon nitride and its sensing for rutin. Anal Chem 85(5):2601–2605. https://doi.org/10.1021/ac303263n
21. Shang QW, Zhou ZX, Shen YF, Zhang YY, Li Y, Liu SQ, Zhang YJ (2015) Potential-modulated electrochemiluminescence of carbon nitride nanosheets for dual-signal sensing of metal ions. ACS Appl Mater Inter 7(42):23672–23678. https://doi.org/10.1021/acsami.5b07405
22. Chen PP, Xia FQ, Tian D, Zhou CL (2018) A dual-coreactants electrochemiluminescent immunosensor for procalcitonin detection based on CdS-MoS2 nanocomposites. J Electrochem Soc 165(5):B196–B201. https://doi.org/10.1149/2.0531805jes
23. Xua HF, Liang SJ, Zhu X, Wu XQ, Dong YQ, Wu HS, Zhang WX, Chi YW (2017) Enhanced electrogenerated chemiluminescence behavior of C_3N_4QDs@C_3N_4 nanosheet and its signal-on aptasensing for platelet derived growth factor. Biosens Bioelectron 92:695–701. https://doi.org/10.1016/j.bios.2016.10.026
24. Zong LY, Zhang GD, Zhao JH, Dong F, Zhang JY, Tang ZC (2018) Morphology-controlled synthesis of 3D flower-like TiO_2 and the superior performance for selective catalytic reduction of NO_x with NH_3. Chem Eng J 343:500–511. https://doi.org/10.1016/j.cej.2018.03.035
25. Wang YZ, Zhao W, Dai PP, Lu HJ, Xu JJ, Pan J, Chen HY (2016) Spatial-resolved electrochemiluminescence ratiometry based on bipolar electrode for bioanalysis. Biosens Bioelectron 86:683–689. https://doi.org/10.1016/j.bios.2016.07.067
26. Sun Y, Zhang YM, Zhang HX, Liu ML, Liu Y (2020) Integrating highly efficient recognition and signal transition of g-C_3N_4 embellished Ti_3C_2 MXene hybrid nanosheets for electrogenerated chemiluminescence analysis of protein kinase. Anal Chem 92:10668–10676. https://doi.org/10.1021/acs.analchem.0c01776
27. Yao Y, Huang XH, Chen Q, Zhang Z, Ling WW (2020) High sensitivity and high stability QCM humidity sensors based on polydopamine coated cellulose nanocrystals/graphene oxide nanocomposite. Nanomaterials 10(11):2210. https://doi.org/10.3390/nano10112210
28. Dengwp ChuCC, Ge SG, Yu JH, Yan M, Song XR (2015) Electrochemiluminescence PSA assay using an ITO electrode modified with gold and palladium, and flower-like titanium dioxide microparticles as ECL labels. Microchim Acta 182(5–6):1009–1016. https://doi.org/10.1007/s00604-014-1423-2
29. Wang YZ, Hao N, Feng QM, Shi HS, Xu JJ, Chen HY (2016) A ratiometric electrochemiluminescence detection for cancer cells using g-C_3N_4 nanosheets and Ag-PAMAM-luminol nanocomposites. Biosens Bioelectron 77:76–82. https://doi.org/10.1016/j.bios.2015.08.057
30. Ou X, Tan XR, Liu XF, Lu QY, Chen SH, Wei SP (2015) A signal-on electrochemiluminescence biosensor for detecting Con A using phenoxy dextran-graphite-like carbon nitride as signal

probe. Biosens Bioelectron 70:89–97. https://doi.org/10.1016/j.bios.2015.03.021
31. Zuo FM, Jin L, Fu XM, Zhang H, Yuan R, Chen SH (2017) An electrochemiluminescent sensor for dopamine detection based on a dual-molecule recognition strategy and polyaniline quenching. Sensor Actuat B-Chem 244:282–289. https://doi.org/10.1016/j.snb.2017.01.001
32. Zhou M, Pu YX, Wu Q, Wang PJ, Liu TT, Zhang MX (2020) 2D hexagonal SnS_2 nanoplates as novel co-reaction accelerator for construction of ultrasensitive g-C_3N_4-based electrochemiluminescent biosensor. Sensor Actuat B-Chem 319:128298. https://doi.org/10.1016/j.snb.2020.128298
33. Yang H, Jin ZL, Hu HY, Lu GX, Bi YP (2017) Fivefold enhanced photoelectrochemical properties of ZnO nanowire arrays modified with C_3N_4 quantum dots. Catalysts 7(4):99. https://doi.org/10.3390/catal7040099
34. Zhen C, Wu TT, MohammadWK II, Liu G, Cheng HM (2015) Design and construction of a film of mesoporous single-crystal rutile TiO_2 rod arrays for photoelectrochemical water oxidation. Chinese J Catal 36(12):2171–2177. https://doi.org/10.1016/S1872-2067(15)60981-0
35. Jimmy CY, Yu JG, Tang HY, Zhang LZ (2002) Effect of surface microstructure on the photoinduced hydrophilicity of porous TiO_2 thin films. J Mater Chem 12:81–85. https://doi.org/10.1039/B102909F
36. Lu XY, Zhang SF, Kong FY, Wang ZX, Li HY, Fang HL, Wang W (2021) Facile synthesis of TiO_2-ZnO-rGO nanocomposites for highly sensitive simultaneous determination of hydroquinone and catechol. Microchem J 166:106246. https://doi.org/10.1016/j.microc.2021.106246
37. Wang ZX, Xing KY, Ding NS, Wang SH, Zhang GG, Lai WH (2021) Lateral flow immunoassay based on dual spectral-overlapped fluorescence quenching of polydopamine nanospheres for sensitive detection of sulfamethazine. J Hazard Mater 423:127204. https://doi.org/10.1016/j.jhazmat.2021.127204
38. Wang H, Pu GQ, Devaramani S, Wang YF, Yang ZF, Li LF, Ma XF, Lu XQ (2018) Bimodal electrochemiluminescence of G-CNQDs in the presence of double coreactants for ascorbic acid detection. Anal Chem 90(7):4871–4877. https://doi.org/10.1021/acs.analchem.8b00517
39. Fan Y, Tan XG, Ou X, Lu QY, Chen SH, Wei SP (2016) A novel "on-off" electrochemiluminescence sensor for the detection of concanavalin A based on Ag-doped g-C_3N_4. Electrochim Acta 202:90–99. https://doi.org/10.1016/j.electacta.2016.04.013
40. Zhang C, Liu D, Zhang H, Tan XR, Chen SH (2019) A ratiometric electrochemiluminescent immunoassay for calcitonin by using N-(aminobutyl)-N-(ethylisoluminol) and graphite-like carbon nitride. Microchim Acta 186(12):771. https://doi.org/10.1007/s00604-019-3934-3
41. Xing YQ, Han J, Wu X, Pierce DT, Zhao JXJ (2020) Graphene/gold nanoparticle composites for ultrasensitive and versatile biomarker assay using single-particle inductively-coupled plasma/mass spectrometry. Analyst 145:7932–7940. https://doi.org/10.1039/D0AN01019G
42. Wang J, Song MM, Hu CG, Wu KB (2018) Portable, self-powered, and light-addressable photoelectrochemical sensing platforms using pH meter readouts for high-throughput screening of thrombin inhibitor drugs. Anal Chem 90:9366–9373. https://doi.org/10.1021/acs.analchem.8b01979
43. Fan TT, Du Y, Yao Y, Wu J, Meng S, Luo JJ, Zhang X, Yang DZ, Wang CY, Qian Y, Gao FL (2018) Rolling circle amplification triggered poly adenine-gold nanoparticles production for label-free electrochemical detection of thrombin. Sensor Actuat B-Chem 266:9–18. https://doi.org/10.1016/j.snb.2018.03.112